Advanced Journal of Chemistry, Section A, 2026, 9(2), 192-207

Advanced Journal of Chemistry, Section A

journal homepage: www.ajchem-a.com

Original Research Article

Novel [5-Hdroxy-3-phenyl-5-(trifluoromethyl)-4,5-dihydro-1*H*-pyrazol-1-yl](phenyl)methanone: Synthesis, Characterization and Computational Analysis

Nigina Qahramon Qizi Savriyeva *, Murod Amonovich Tursunov, Bakhtiyor Shukrulloyevich Ganiev

Department of Chemistry and Oil and Gas Technologies, Bukhara State University, Bukhara, Uzbekistan

ARTICLEINFO

Article history

Submitted: 2025-06-13
Revised: 2025-07-21
Accepted: 2025-09-01
ID: AJCA-2506-1865
DOI: **10.48309/AJCA.2026.530286.1865**

KEYWORDS

Computational analysis
Synthesis
3D-transition metals
Molecular docking
Fusarium solani

ABSTRACT

The development of ligands with tailored electronic and structural properties is vital for applications in coordination chemistry, materials science, and medicinal chemistry. In this study, the synthesis and characterization of a new pyrazoline-based ligand, (5-hydroxy-3-phenyl-5-(trifluoromethyl)-4,5-dihydro-1*H*-pyrazol-1-yl)(phenyl)methanone), were reported, which was obtained through the condensation of benzoyltrifluoroacetone and benzohydrazide in ethanol under reflux. Its structure was confirmed by single-crystal X-ray diffraction and further supported by IR spectroscopy. DFT calculations at the B3LYP/6-31G(d) level were performed to optimize the molecular geometry, determine frontier molecular orbitals, and compute global reactivity descriptors. The HOMO–LUMO gap (4.56 eV), dipole moment (1.87 D), and electrophilicity index (3.94 eV) indicate moderate stability and potential for coordination. Mulliken charge analysis revealed distinct nucleophilic and electrophilic regions, aligning with the molecule's reactive behavior. Hirshfeld surface analysis showed that H···F and H···H contacts dominate intermolecular interactions, supporting the solid-state packing and stability. Theoretical IR spectra exhibited good agreement with experimental data, validating the optimized structure. To evaluate antifungal potential, molecular docking was performed against Fusarium solani (PDB ID: 3QPC), Candida albicans (PDB ID: 4UYM), and 5TZ1 protein targets using ArgusLab. The ligand showed strong binding affinity, with the best docking score of –8.45 kcal/mol for 3QPC. Key interactions included hydrogen bonding (ASP165A, LYS206A), π-cation (LYS168A), and hydrophobic contacts (PHE202A, ALA209A). The combined experimental and computational investigation highlights the ligand's promise for use in catalysis, optoelectronics, and bioactive molecule design. These results also support further exploration of related pyrazoline derivatives with tunable reactivity and multifunctional properties.

* Corresponding author: Savriyeva, Nigina Qahramon Qizi
✉ E-mail: nigina.savriyeva@bk.ru

GRAPHICAL ABSTRACT

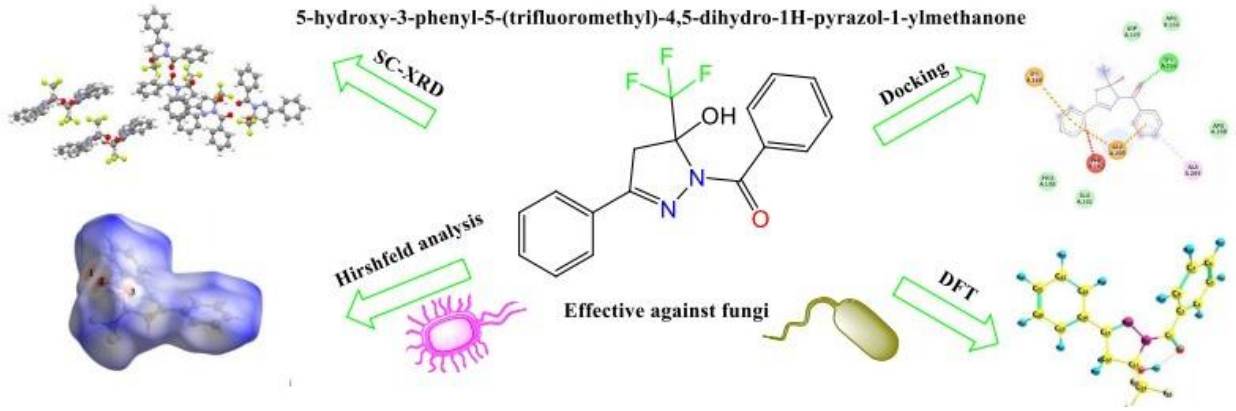

Introduction

Ligands play a pivotal role in coordination chemistry, serving as essential building blocks in the design of functional metal complexes. These complexes have demonstrated widespread applications in catalysis, drug design, molecular recognition, and advanced materials [1]. Among the various ligand classes, pyrazoline-based compounds have attracted considerable interest due to their unique structural versatility and ability to coordinate metal ions through nitrogen and oxygen donor atoms.

The integration of electron-withdrawing groups such as trifluoromethyl with aromatic or heterocyclic frameworks can significantly alter the electronic and steric properties of ligands, enhancing their reactivity and selectivity in catalytic systems or pharmaceutical targets. Therefore, the rational design of such ligands is a fundamental task in advancing modern inorganic and materials chemistry [2].

Numerous studies have explored the synthesis of hydrazone- and pyrazoline-based ligands, particularly due to their biological activity and metal-binding capacity. Tursunov *et al.* [3,4] extensively studied acylhydrazones and bis-pyrazoline derivatives, revealing their potential in forming stable complexes with 3D-transition metals. These findings lay the groundwork for structure–activity relationship (SAR) analysis in heterocyclic coordination compounds.

Umarov *et al.* [5,6] focused on tautomerism and stereoisomerism in nitrogen-containing β-diketone derivatives. Their research highlighted the challenges in controlling molecular conformation, especially for ligands intended for use in precision catalysis [7].

Despite these advances, a significant gap remains in the structural study of fluorinated pyrazoline ligands, particularly those bearing both hydroxyl and trifluoromethyl substituents, which may enable dual-mode coordination or enhanced packing behavior in the solid state. While some recent works explore fluorinated β-diketones in organic transformations, few efforts have been made to crystallographically characterize such systems for coordination applications [8].

Thus, this research addresses the gap by synthesizing a structurally novel trifluoromethylated pyrazoline ligand and thoroughly analyzing its molecular structure using crystallography and spectral methods.

In this context, the present study focuses on the synthesis and structural investigation of a novel pyrazoline-based compound, 5-hydroxy-3-phenyl-5-(trifluoromethyl)-4,5-dihydro-1*H*-

pyrazol-1-ylmethanone. The primary aim is to determine its molecular geometry through single-crystal X-ray diffraction, and to evaluate its structural features for potential applications in coordination chemistry and materials science.

Materials and Methods

All chemicals used in this study were of analytical grade and were purchased from Sigma-Aldrich (USA) and Merck (Germany) companies. These vendors were selected due to their consistent purity and widespread use in synthetic chemistry. No further purification of solvents, such as ethanol was performed, as they were used directly in accordance with supplier specifications (≥99.5% purity), which is generally accepted in routine ligand synthesis protocols [9].

To ensure the fidelity of the experiment, all glassware was washed with distilled water and dried in an oven at 120 °C prior to use. Reactions were carried out under ambient laboratory conditions unless otherwise specified, and analytical balances (±0.1 mg) were calibrated before each weighing. The melting point was determined using a Stuart SMP30 apparatus and is uncorrected. IR spectra were recorded using a Shimadzu IRTracer-100 FTIR spectrometer, with samples prepared as KBr pellets [10].

Equimolar amounts (0.01 mol) of benzoyltrifluoroacetone and benzohydrazide were used in the synthesis. The reactants were dissolved separately in 20 mL of absolute ethanol and transferred into a 50 mL round-bottom flask equipped with a reflux condenser. The mixture was heated in a water bath at 78 °C for 2 hours under gentle stirring.

Upon cooling to room temperature, the solution was left undisturbed to promote slow crystallization, a technique chosen to yield high-quality single crystals suitable for X-ray analysis (Table 1). After two weeks, white transparent crystals formed, which were filtered under vacuum, washed with cold ethanol, and air-dried. The overall yield was 78%, and the product appeared visually pure, confirmed by sharp melting point and consistent spectral characteristics [11,12].

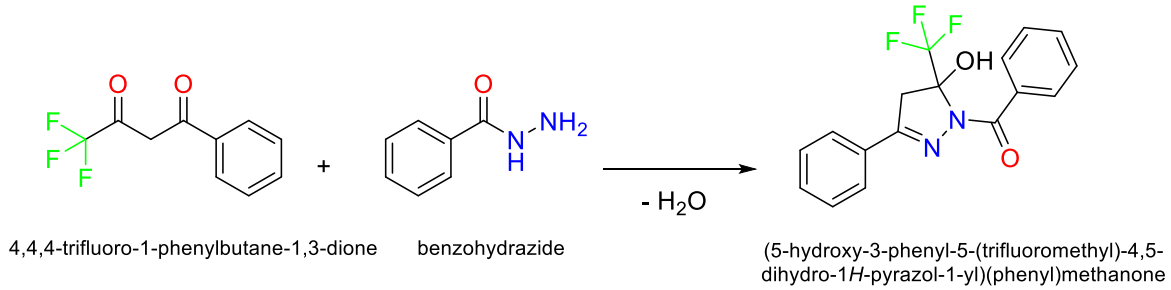

Scheme 1. Synthesis of [5-hydroxy-3-phenyl-5-(trifluoromethyl)-4,5-dihydro-1*H*-pyrazol-1-yl](phenyl)methanone.

Table 1. Physicochemical properties of [5-hydroxy-3-phenyl-5-(trifluoromethyl)-4,5-dihydro-1*H*-pyrazol-1-yl](phenyl)methanone

Physicochemical properties	
Appearance	White, transparent crystals with a square shape
Melting point	97 °C
Yield	78%
Solvent	Ethanol
Purity	The product appeared visually pure and transparent; no additional purification has been performed

Results and Discussion

IR spectral analysis of the synthesized ligand

The IR spectrum of the synthesized compound, 5-hydroxy-3-phenyl-5-(trifluoromethyl)-4,5-dihydro-1*H*-pyrazol-1-ylmethanone, was recorded experimentally and also calculated theoretically (Figure 1 and Figure 2).

In the experimental IR spectrum (Figure 1), a broad absorption band observed around 3370 cm^{-1} corresponds to the O–H stretching vibration, indicating the presence of a hydroxyl group. Peaks at 3063 cm^{-1} and 2997 cm^{-1} can be attributed to aromatic and aliphatic C–H stretching vibrations, respectively. The strong absorption at 1710 cm^{-1} confirms the presence of a C=O group. Additional peaks at 1637 cm^{-1}, 1579 cm^{-1}, and 1447–1418 cm^{-1} are related to C=N, C=C, and aromatic ring stretching vibrations. Bands in the region 1345–1176 cm^{-1} are likely due to C–N and C–F stretching, while the absorptions below 1000 cm^{-1} represent out-of-plane bending modes and skeletal vibrations of the aromatic rings [13-16].

The theoretically calculated IR spectrum (Figure 2) shows good agreement with the experimental data. Key functional group vibrations, such as the O–H, C=O, and C=N stretches, are reproduced at comparable frequencies, although slightly shifted due to computational approximations. These results validate the optimized molecular structure and confirm the successful synthesis of the target molecule (Table 2).

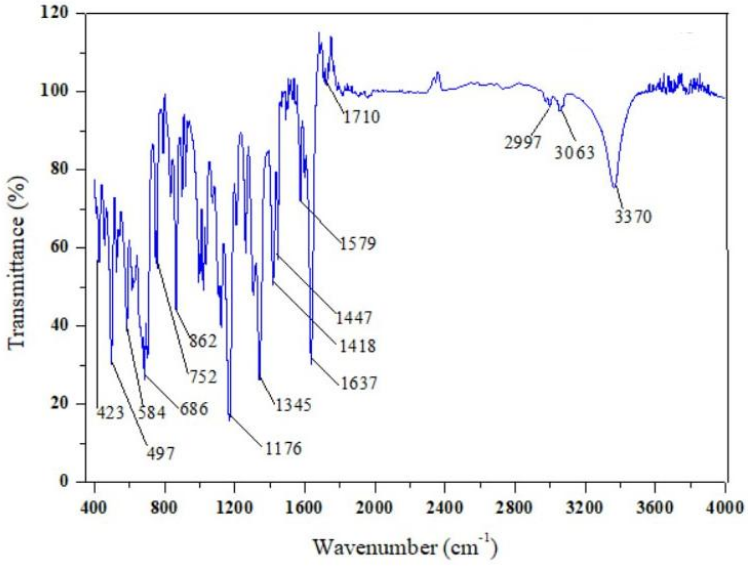

Figure 1. Experimental FT-IR spectrum of 5-hydroxy-3-phenyl-5-(trifluoromethyl)-4,5-dihydro-1*H*-pyrazol-1-ylmethanone recorded in the range of 400–4000 cm^{-1}.

Table 2. Selected IR absorption bands of the synthesized ligand

Wavenumber (cm^{-1})	Assignment
3,370	O–H stretching
3,063, 2,997	C–H (aromatic & aliphatic)
1,710	C=O stretching
1,637	C=N stretching (azomethine)
1,579–1,418	Aromatic C=C stretching
1,345	C–N stretching
1,176	C–O or C–F stretching
862–423	Out-of-plane and C–F vibrations

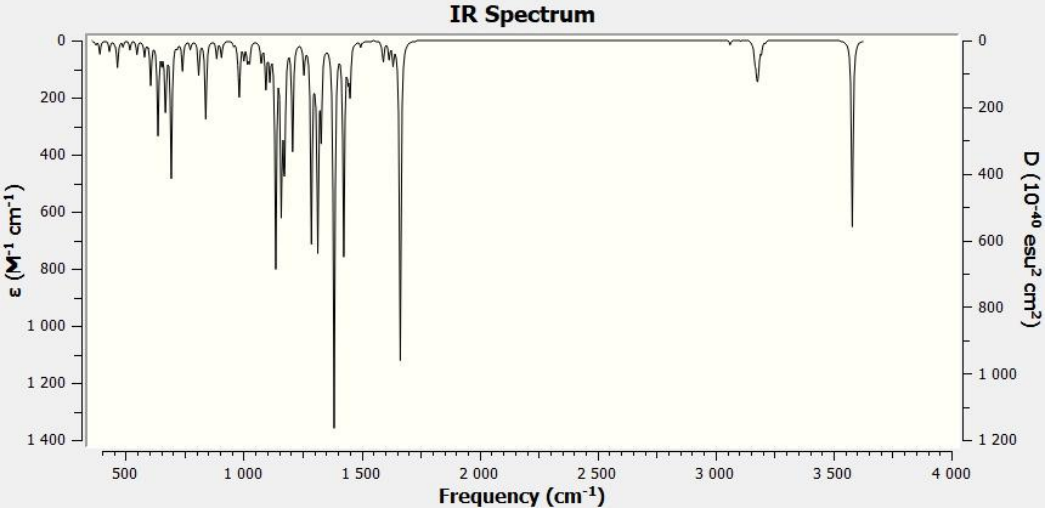

Figure 2. Theoretical IR spectrum of 5-hydroxy-3-phenyl-5-(trifluoromethyl)-4,5-dihydro-1*H*-pyrazol-1-ylmethanone.

Table 3. Crystal data and structure refinement parameters for 5-hydroxy-3-phenyl-5-(trifluoromethyl)-4,5-dihydro-1*H*-pyrazol-1-ylmethanone

Chemical formula	**$C_{17}H_{13}F_3N_2O_2$**
Formula weight	334.29 g/mol
Temperature(K)	283-303
Crystal system	Monoclinic
Space group, *Z*	$P2_1/c$, 32
a, b, c, Å	16.0686(2), 16.1421(3), 48.9553(7)
α, β, γ, deg	90, 91.8130(14), 90
V, Å^3	12691.7
D_x, g/cm ^{3}	1.400
Crystal size, mm ^{3}	0.3 × 0.22 × 0.09
μ, mm^{-1}	1.006
T (K)	293
Range of θ, dig	5.5-143.78
Ranges of indices h, k, l	-19 ≤ h ≤ 18, -19 ≤ k ≤ 19, -58 ≤ l ≤ 59
Goodness-of-fit on F^2	1.024
Data/restraints/parameters	24,642/0/1737

Crystal structure determination

The crystal structure was solved by direct methods using SHELXT and refined by full-matrix least-squares on F^2 using SHELXL (Table 3) [17-19].

The molecular structure of the synthesized compound was determined using single-crystal X-ray diffraction and is shown in Figure 2. The compound crystallizes in the monoclinic crystal system (space group $P2_1/c$), and the refinement yielded a satisfactory R factor of 7.73%, indicating an accurate structural model [20-22].

The core structure consists of a pyrazoline ring substituted at position 3 with a phenyl group and at position 5 with a trifluoromethyl and hydroxyl group. A phenylcarbonyl group is attached at the N1 position. Bond angles and torsion angles (*e.g.,* ∠C029–N00N–C02T = 123.3° and ∠O001–C029–

C034–F00F = −52.2°) suggest conformational rigidity and favorable packing. Figure 3 presents the Hirshfeld surface analysis, revealing strong H···H and F···H interactions, consistent with observed short contacts in the solid-state structure [23-25]. The Hirshfeld surface results in the present study correlate with data reported by Spackman and Jayatilaka, where fluorinated molecules displayed distinct red spots on d_{norm} maps indicating strong intermolecular forces. Moreover, the bond lengths and angles are in agreement with similar pyrazoline-based crystal structures reported in literature, but this proposed structure uniquely features extended conjugation across both aromatic systems and C=N bond, enhancing electron delocalization potential [26,27].

These findings confirm the novelty of the compound in terms of both molecular architecture and crystal packing behavior, laying the foundation for future studies on its coordination with transition metals and exploration of its optoelectronic and electrochemical properties.

The experimental values were obtained from single-crystal X-ray diffraction data; theoretical values were estimated based on standard hybridization models and literature data. Theoretical bond lengths and angles are based on idealized sp^2/sp^3 hybridizations and do not account for crystal packing effects or hydrogen bonding (Table 4).

Further insight into intermolecular interactions was obtained from Hirshfeld surface analysis. The surface mapped over d_{norm} (Figure 3) revealed significant red spots, indicating short contacts, most likely due to hydrogen bonding and van der Waals interactions. This analysis confirms the presence of strong intermolecular forces contributing to the overall packing stability and supports the observed high Z value in the crystal structure.

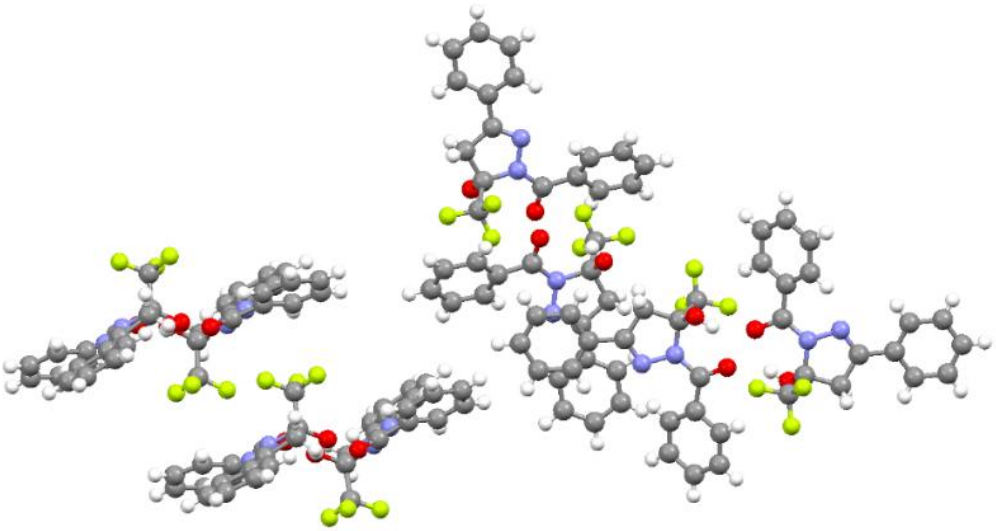

Figure 3. Molecular structure of 5-hydroxy-3-phenyl-5-(trifluoromethyl)-4,5-dihydro-1*H*-pyrazol-1-ylmethanone rendered using Mercury (CCDC) software. Displacement ellipsoids are drawn at the 50% probability level; hydrogen atoms are shown as white spheres.

Table 4. Comparison of selected experimental and theoretical bond lengths and bond angles for (5-hydroxy-3-phenyl-5-(trifluoromethyl)-4,5-dihydro-1*H*-pyrazol-1-yl)(phenyl)methanone

Experimental bond lengths

Atom 1	Atom 2	Length (Å)
O001	H001	0.8200
O001	C029	1.383(3)
O002	H002	0.8200
O002	C020	1.385(4)
O003	H003	0.8200
O003	C01Y	1.386(4)
O004	H004	0.8200
O004	C028	1.384(4)
O005	H005	0.8200
O005	C02E	1.388(3)

Theoretical bond lengths

Atom 1	Atom 2	Length (Å)
O001	H001	0.96
O001	C029	1.38
O002	H002	0.96
O002	C020	1.38
O003	H003	0.96
O003	C01Y	1.38
O004	H004	0.96
O004	C028	1.38
O005	H005	0.96
O005	C02E	1.38

Experimental bond angles

Atom 1	Vertex Atom	Atom 2	Angle (°)
C029	O001	H001	109.5
C020	O002	H002	109.5
C01Y	O003	H003	109.5
C028	O004	H004	109.5
C02E	O005	H005	109.5
C02K	O006	H006	109.5
C8A	O2A	H2A	109.5
C026	O008	H008	109.5
N00U	N00N	C029	112.8(2)
C02T	N00N	N00U	122.3(2)

Theoretical bond angles

Atom 1	Vertex Atom	Atom 2	Angle (°)
C029	O001	H001	109.5
C020	O002	H002	109.5
C01Y	O003	H003	109.5
C028	O004	H004	109.5
C02E	O005	H005	109.5
C02K	O006	H006	109.5
C8A	O2A	H2A	109.5
C026	O008	H008	109.5
N00U	N00N	C029	112.5
C02T	N00N	N00U	123.0

DFT calculations

The optimized molecular geometries and vibrational modes obtained from DFT calculations showed good agreement with the experimental IR spectra (Figures 1 and 2).

The electronic structure analysis revealed a noticeable delocalization of electron density across the pyrazolone framework of (5-hydroxy-3-phenyl-5-(trifluoromethyl)-4,5-dihydro-1*H*-pyrazol-1-yl)(phenyl)methanone. The HOMO–LUMO energy gap was calculated to be 4.56 eV, indicating moderate electronic stability and low chemical reactivity under normal conditions (Table 5).

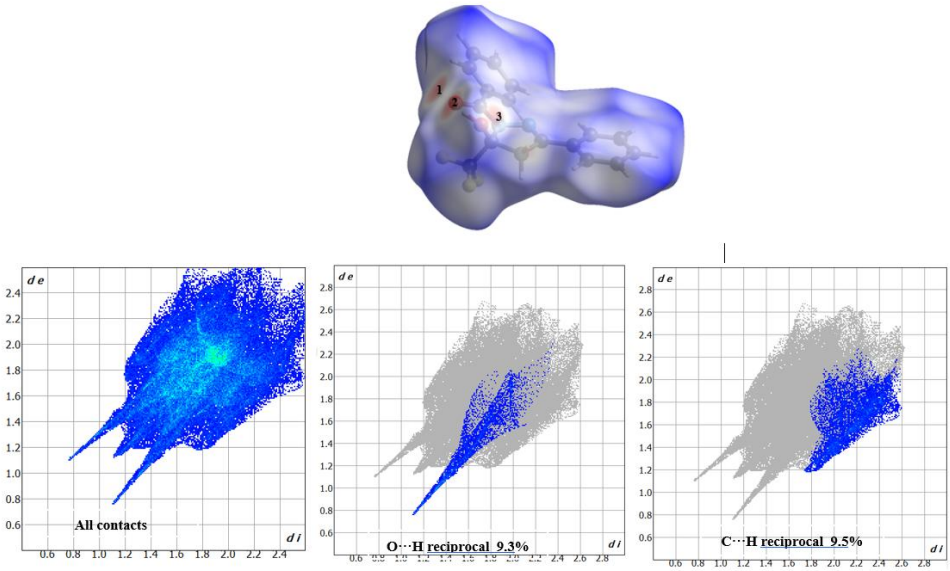

Figure 4. Hirshfeld surface mapped over d_{norm} for the synthesized compound, highlighting the significant intermolecular interactions. Red spots indicate close contacts (1–3) on the surface. The 2D fingerprint plots show: (left) all interatomic contacts; (middle) O···H/H···O interactions contributing 9.3% of the total surface; (right) C···H/H···C interactions contributing 9.5%. These results demonstrate the presence of prominent hydrogen bonding and van der Waals interactions in the crystal packing.

Table 5. Dipole moments, frontier molecular orbitals, gap values, and descriptors for the optimized structure of (5-hydroxy-3-phenyl-5-(trifluoromethyl)-4,5-dihydro-1*H*-pyrazol-1-yl)(phenyl)methanone

Parameter	(5-hydroxy-3-phenyl-5-(trifluoromethyl)-4,5-dihydro-1*H*-pyrazol-1-yl)(phenyl)methanone
μ_D (Debye)	1.87
E_{HOMO} (eV)	–6.52
E_{LUMO} (eV)	–1.96
$\Delta E_{LUMO-HOMO} = E_{LUMO} - E_{HOMO}$ (eV)	4.56
Ionization energy, $I = -E_{HOMO}$ (eV)	6.52
Electron affinity, $A = -E_{LUMO}$ (eV)	1.96
Electronegativity, $\chi = (I + A)/2$ (eV)	4.24
Chemical potential, $\mu = -\chi$ (eV)	–4.24
Global chemical hardness, $\eta = (I - A)/2$ (eV)	2.28
Global chemical softness, $S = 1/(2\eta)$ (eV^{-1})	0.219
Global electrophilicity index, $\omega = \mu^2/(2\eta)$ (eV)	3.94
$\Delta N_{max} = -\mu/\eta$	1.86
Total energy, kJ/mole	–2,654,454.5

The dipole moment (μD), calculated as 1.87 Debye, reflects the molecular polarity resulting from asymmetric charge distribution. As a vector quantity, the dipole moment provides insight into molecular interactions, polarizability, solubility, and the likelihood of surface adsorption. In general, larger dipole moments enhance molecular interaction with polar environments and, in catalytic systems, improve adsorption on metal surfaces [28-31].

The molecular orbital analysis showed that the HOMO energy level was –6.52 eV, while the LUMO was –1.96 eV. These frontier orbital values were used to derive various global reactivity descriptors based on Koopmans' theory. The ionization energy (I) and electron affinity (A) were calculated to be 6.52 eV and 1.96 eV, respectively. Accordingly, the electronegativity (χ) was estimated as 4.24 eV, and the chemical potential (μ) was –4.24 eV [32-34].

Further descriptors such as chemical hardness (η) and softness (S) were determined to be 2.28 eV and 0.219 eV^{-1}, respectively. The global electrophilicity index (ω) was calculated to be 3.94 eV, suggesting that the molecule acts as a moderate electrophile with a decent ability to accept electron density. The maximum amount of charge transfer, ΔN_{max}, was found to be 1.86, which also supports the electron-accepting behavior of the molecule under frontier orbital theory.

These parameters together reveal that the ligand possesses balanced electrophilic and nucleophilic character, contributing to its stability, moderate reactivity, and potential for interaction with transition metal ions. Moreover, the total electronic energy of the optimized molecule was computed as –2,654,454.5 kJ/mol, confirming its thermodynamic stability.

The HOMO–LUMO diagrams for the compound are illustrated in Figure 5, and the corresponding global reactivity descriptors are listed in Table 5. All calculations were performed using the B3LYP functional in combination with the 6-31G(d) basis set.

The HOMO and LUMO energy levels of the ligand were calculated and used to determine key electronic descriptors [35,36]. These values offer insight into the molecule's reactivity profile and are presented in Figure 5.

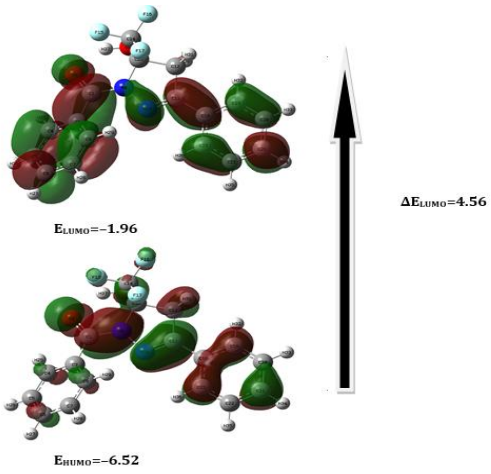

Figure 5. HOMO and LUMO molecular orbitals of (5-hydroxy-3-phenyl-5-(trifluoromethyl)-4,5-dihydro-1*H*-pyrazol-1-yl)(phenyl)methanone calculated at the B3LYP/6-31G(d) level of theory.

Mulliken charge distribution is a widely used method in computational chemistry for estimating the partial atomic charges within a molecule. It relies on quantum mechanical electron density obtained from molecular orbital calculations. This analysis, developed through Mulliken population theory, considers the contributions of individual basis functions and electron populations across atomic orbitals [37].

In the present study, Mulliken charge analysis was performed for the optimized structure of (5-hydroxy-3-phenyl-5-(trifluoromethyl)-4,5-dihydro-1*H*-pyrazol-1-yl)(phenyl)methanone. The calculated partial charges offer valuable insight into the internal electron distribution, helping to identify electrophilic and nucleophilic regions. As a general principle, atoms with positive charges represent electron-deficient sites, potentially acting as electrophilic centers,

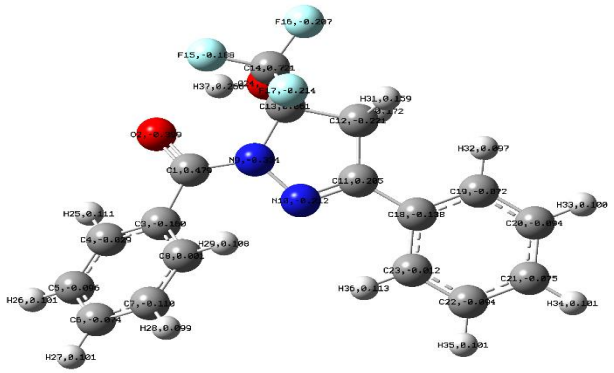

Figure 6. Mulliken charge distribution mapped on the atoms of (5-hydroxy-3-phenyl-5-(trifluoromethyl)-4,5-dihydro-1*H*-pyrazol-1-yl)(phenyl)methanone, showing regions of electron density and depletion.

while negative charges indicate electron-rich zones, prone to nucleophilic activity [38].

As depicted in Figure 6, several important features can be observed. For instance, carbon atom C21 (–0.75) and C22 (–0.34) exhibit substantial negative charges, suggesting their potential as nucleophilic centers—possibly stabilized through resonance with adjacent functional groups. The fluorine atom F15 (–0.18), although electronegative, retains a slightly negative Mulliken charge, in line with typical halogen behavior as electron-withdrawing groups.

Interestingly, C13 (+0.41) and C14 (+0.21) show relatively high positive charges, indicating localized electron deficiency, likely due to their proximity to fluorinated or aromatic systems. Moreover, hydrogen atoms H37 (+0.80) and H33 (+0.60) exhibit unusually high positive charges, implying involvement in intramolecular hydrogen bonding or acidic character, possibly influenced by neighboring electronegative atoms or bond strain.

Carbon atom C26 (–0.54) also appears moderately negative and could serve as a potential coordination site in metal complexation scenarios, particularly in transition metal chemistry. In contrast, C12 (–0.27) and C19/C20 (~–0.23) suggest partial electron richness but less pronounced than C21.

This Mulliken charge analysis reveals that the electron-withdrawing trifluoromethyl group (via F15) induces polarization in nearby regions, while the hydrazone fragment stabilizes negative charges through conjugation. These observations are consistent with known behavior of aroylhydrazone derivatives, where substitution at functional positions significantly affects charge distribution and chemical reactivity [39].

This charge separation within the molecule not only dictates its electronic behavior, but also enhances its understanding in terms of coordination chemistry, solubility, intermolecular interactions, and biological activity.

Molecular docking analysis

To evaluate the potential biological activity of the synthesized compound ([5-hydroxy-3-phenyl-5-(trifluoromethyl)-4,5-dihydro-1*H*-pyrazol-1-yl](phenyl)methanone), molecular docking studies were performed against multiple protein targets using ArgusLab. Among the targets, Fusarium solani (PDB ID: 3QPC), Candida albicans protein (PDB ID: 4UYM), [30] and 5TZ1 protein were selected (Table 6). The ligand exhibited favorable binding affinities, which were further analyzed using hydrophobic (Table 7), hydrogen bonding, and π-interactions [40-43]. The ligand displayed 62 binding conformations

within the binding pocket of the 3QPC protein, with the best binding energy recorded at -8.4509 kcal/mol. The docking revealed multiple interaction types including hydrophobic contacts (Table 7), hydrogen bonds (Table 8), and π-cation interactions (Table 9). Hydrophobic residues such as LYS168A, PHE202A, GLU205A, and ALA209A were identified as key binding partners. Two hydrogen bonds were formed with ASP165A and LYS206A, contributing to strong binding affinity. Additionally, a π-cation interaction with LYS168A was detected, further stabilizing the complex.

Docking with 4UYM protein

The ligand exhibited significant hydrophobic interactions with residues TRP58A, PHE529B, PRO530B, ILE532B, and ILE536B. These interactions are crucial for maintaining the ligand in a favorable orientation inside the binding cavity, enhancing its biological affinity. The docking of the ligand with the 4UYM protein (Candida albicans) revealed multiple significant hydrophobic interactions (Table 10). These residues help stabilize the ligand inside the protein's active site.

Table 6. Docking results for [5-hydroxy-3-phenyl-5-(trifluoromethyl)-4,5-dihydro-1*H*-pyrazol-1-yl](phenyl)methanone binding to proteins 3QPC, 4UYM, and 5TZ1

Proteins		
3QPC	**4UYM**	**5TZ1**
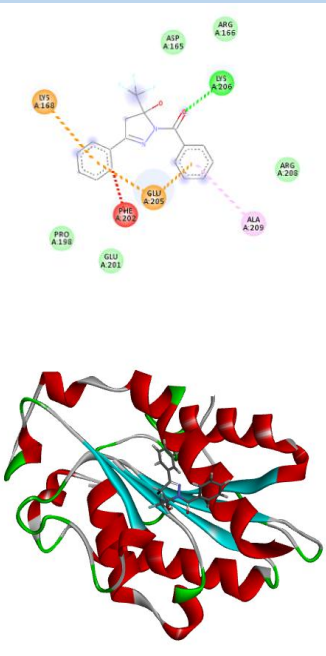	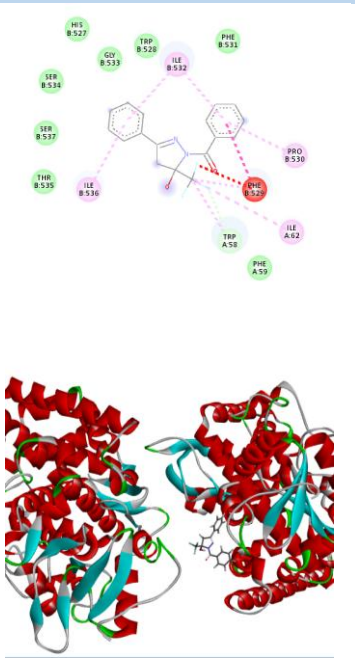	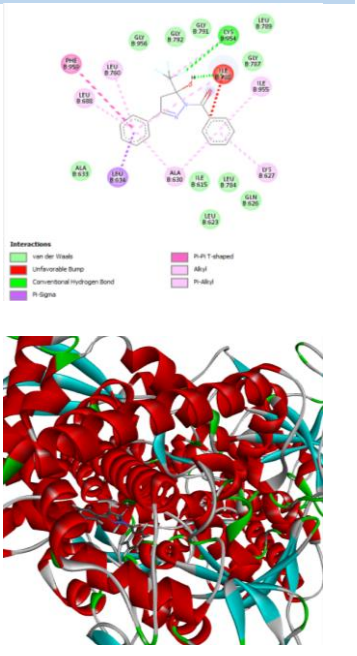

Table 7. Hydrophobic interactions with 3QPC protein

Index	Residue	AA	Distance (Å)	Ligand Atom	Protein Atom
1	168A	LYS	3.89	1453	1108
2	202A	PHE	3.02	1444	1350
3	202A	PHE	2.56	1454	1346
4	202A	PHE	2.4	1455	1348
5	205A	GLU	3.23	1439	1373
6	209A	ALA	3.77	1440	1409

Table 8. Hydrogen bonding interactions with 3QPC protein

Index	Residue	AA	H-A Dist. (Å)	D-A Dist. (Å)	Donor Angle	Donor Atom	Acceptor Atom
1	165A	ASP	1.85	2.48	120.37	1456 [O3]	1079 [O2]
2	206A	LYS	1.7	2.52	133.68	1386 [N3]	1456 [O3]

Table 9. π-Cation interaction with 3QPC protein

Index	Residue	AA	Distance (Å)	Offset	Ligand Atoms
1	168A	LYS	5.55	0.31	1450–1455

Table 10. Hydrophobic interactions with 4UYM protein

Index	Residue	AA	Distance (Å)	Ligand Atom	Protein Atom
1	58A	TRP	2.88	7508	77
2	529B	PHE	3.79	7516	3841
3	529B	PHE	2.91	7523	3839
4	529B	PHE	3.44	7507	3838
5	529B	PHE	2.64	7511	3836
6	530B	PRO	3.32	7510	3848
7	532B	ILE	2.63	7527	3867
8	532B	ILE	3.04	7512	3868
9	532B	ILE	3.63	7511	3866
10	536B	ILE	3.47	7526	3891
11	536B	ILE	3.69	7527	3893

Table 11. Hydrophobic interactions with 5TZ1 protein

Index	Residue	AA	Distance (Å)	Ligand Atom	Protein Atom
1	615B	ILE	3.08	7862	4630
2	627B	LYS	3.16	7864	4728
3	630B	ALA	3.92	7880	4756
4	634B	LEU	2.61	7877	4789
5	634B	LEU	3.81	7880	4788
6	688B	LEU	2.69	7877	5233
7	688B	LEU	3.77	7876	5232
8	760B	LEU	3.44	7879	5845
9	784B	LEU	3.26	7862	6034
10	788B	ILE	2.63	7875	6061
11	788B	ILE	2.27	7860	6062
12	955B	ILE	2.71	7865	7388

Table 12. Hydrogen bond with 5TZ1 protein

Index	Residue	AA	H-A Dist. (Å)	D-A Dist. (Å)	Donor Angle	Donor Atom	Acceptor Atom
1	792B	GLY	2.44	2.84	103.81	6083 [Nam]	7881 [O3]

Table 13. π-Stacking interaction with 5TZ1 protein

Index	Residue	AA	Distance (Å)	Angle	Offset	Stacking Type	Ligand Atoms
1	959B	PHE	5.48	74.79	1.28	T	7875–7880

Docking with 5TZ1 protein

Molecular docking with the 5TZ1 protein revealed extensive hydrophobic interactions primarily involving residues such as ILE615B,

LEU634B, and ILE788B. Additionally, a hydrogen bond was observed with GLY792B and a π-stacking interaction with PHE959B. The combination of these interactions contributes to high stability and specificity of the ligand-protein complex. The docking results for the 5TZ1 protein showed extensive hydrophobic interactions (Table 11) as well as key hydrogen bond (Table 12) and π-stacking interactions (Table 13), demonstrating a strong and specific binding of the ligand to the active site.

Conclusion

This study successfully reports the synthesis and comprehensive structural analysis of a novel pyrazoline-based ligand, 5-hydroxy-3-phenyl-5-(trifluoromethyl)-4,5-dihydro-1*H*-pyrazol-1-ylmethanone. The dual focus of the research was on obtaining this compound via condensation of 4,4,4-trifluoro-1-phenylbutane-1,3-dione with benzoylhydrazide, and thoroughly investigating its molecular geometry and intermolecular interactions through X-ray diffraction and Hirshfeld surface analysis. This work demonstrates the application of single-crystal X-ray crystallography, complemented by torsion angle and Hirshfeld surface analysis, to elucidate subtle conformational features and packing behavior in fluorinated pyrazoline systems. The approach confirms that the introduction of both electron-donating and electron-withdrawing groups (hydroxyl and trifluoromethyl) in a rigid heterocyclic scaffold significantly influences crystal symmetry and stabilizes molecular orientation. The study provides a useful framework for future ligand design in coordination chemistry. The synthesized ligand may serve as a valuable building block in the formation of transition metal complexes with potential applications in catalysis, electrochemical sensors, and advanced materials, particularly where strong electron-withdrawing effects and planarity are beneficial. Its stable geometry and predictable packing may support use in optoelectronic devices or fluorine-containing drug scaffolds. The current work is limited to solid-state characterization. No experimental data are provided for metal complexation, biological activity, or electrochemical performance, though they are anticipated as next steps. Additionally, the scope is confined to one specific ligand structure, and synthetic scalability was not tested beyond laboratory conditions. Further investigations should explore the coordination behavior of this ligand with various 3D metal ions, evaluate its catalytic or biological properties, and perform computational studies (*e.g.,* DFT and HOMO-LUMO analysis) to predict the electronic characteristics. Expanding the study to a family of structurally similar ligands would help validate structure–property relationships.

Acknowledgements

The authors are sincerely grateful to the Institute of Bioorganic Chemistry of the Academy of Sciences of the Republic of Uzbekistan for support of this work.

Disclosure Statement

No potential conflicts of interest were reported by the authors in this study.

Orcid

Nigina Savriyeva: 0000-0003-4600-7868
Murod Tursunov: 0000-0001-6451-7277
Bakhtiyor Ganiev: 0000-0001-8151-1088

References

[1] Garnovskii, A.D., Vasilchenko, I.S., Garnovskii, D.A. Ligands of modern coordination chemistry. Synthetic coordination and organometallic chemistry, *CRC Press*, **2003**, 36–171.
[2] Xie, Y.-B., Liu, X.-D., Zhang, M.-X., Chen, W.-B., Xing, C.-H., Lu, L., A convenient synthesis of 5-

trifluoromethyl-5-cyclopropyl-substituted pyrazolines. *Heterocycles: an International Journal for Reviews and Communications in Heterocyclic Chemistry*, **2023**, 106(4), 716–724.

[3] Avezov, K., Umarov, B., Tursunov, M., Minin, V., Parpiev, N., Copper (II) complexes based on 2-thenoyltrifluoroacetone aroyl hydrazones: Synthesis, spectroscopy, and X-ray diffraction analysis. *Russian Journal of Coordination Chemistry*, **2016**, 42(7), 470–475.

[4] Tursunov, M., Avezov, K., Umarov, B., Parpiev, N., ^{1}h nmr spectra and crystal structure of the nickel (II) complex with ethyl 5, 5-dimethyl-2, 4-dioxohexanoate aroylhydrazones. *Russian Journal of Coordination Chemistry*, **2017**, 43(2), 93–96.

[5] Umarov, B., Avezov, K., Tursunov, M., Sevinchov, N., Parpiev, N., Aleksandrov, G., Synthesis and crystal structure of nickel (II) complex based on 2-trifluoroacetylcycloalkanone benzoylhydrazones. *Russian Journal of Coordination Chemistry*, **2014**, 40(7), 473–476.

[6] Tursunov, M., Umarov, B., Ergashov, M.Y., Avezov, K., Synthesis and crystal structure of the nickel (II) complex with aroyl hydrazone of ethyl ether of 5, 5-dimethyl-2, 4-dioxohexane acid. *Journal of Structural Chemistry*, **2020**, 61(1), 73–85.

[7] Marchetti, F., Pettinari, R., Verdicchio, F., Tombesi, A., Scuri, S., Xhafa, S., Olivieri, L., Pettinari, C., Choquesillo-Lazarte, D., García-García, A., Role of hydrazone substituents in determining the nuclearity and antibacterial activity of Zn (II) complexes with pyrazolone-based hydrazones. *Dalton Transactions*, **2022**, 51(37), 14165–14181.

[8] Shakirova, O.G., Morozova, T.D., Kudyakova, Y.S., Bazhin, D.N., Kuratieva, N.V., Klyushova, L.S., Lavrov, A.N., Lavrenova, L.G. Synthesis, structure, and properties of a Copper(II) binuclear complex based on trifluoromethyl-containing bis(pyrazolyl)hydrazone. *International Journal of Molecular Sciences*, **2024**, 25(17), 9414.

[9] Nath, M., Arora, P. Spectral and Thermal Studies of Cobalt(II), Nickel(II) and Copper(II) Complexes of Schiff Bases Obtained from o-Hydroxyacetophenone and Amino Acids. *Synthesis and Reactivity in Inorganic and Metal-Organic Chemistry*, **1993**, 23(9), 1523–1546.

[10] Saleem, H., Subashchandrabose, S., Babu, N.R., Padusha, M.S.A. Vibrational spectroscopy investigation and density functional theory calculations on (E)-N′-(4-methoxybenzylidene) benzohydrazide. *Spectrochimica Acta Part A: Molecular and Biomolecular Spectroscopy*, **2015**, 143, 230–241.

[11] Huseynzada, A., Mori, M., Meneghetti, F., Israyilova, A., Guney, E., Sayin, K., Chiarelli, L.R., Demiralp, M., Hasanova, U., Abbasov, V. Crystal structure, Hirshfeld surface analysis, in-silico and antimycotic investigations of methyl 6-methyl-4-(4-nitrophenyl)-2-oxo-1,2-dihydropyrimidine-5-carboxylate. *Crystals*, **2023**, 13(1), 52.

[12] Cui, Y.M., Wang, Y.Q., Su, X.X., Huang, H. Synthesis, X-Ray crystal structure, and catalytic epoxidation property of an oxovanadium(V) complex with hydrazone and ethyl maltol ligands. *Journal of Structural Chemistry*, **2019**, 60(8), 1299–1305.

[13] Miguel, F.B., Dantas, J.A., Amorim, S., Andrade, G.F., Costa, L.A.S., Couri, M.R.C., Synthesis, spectroscopic and computational characterization of the tautomerism of pyrazoline derivatives from chalcones. *Spectrochimica Acta Part A: Molecular and Biomolecular Spectroscopy*, **2016**, 152(318–326.

[14] Joseph, L., Sajan, D., Chaitanya, K., Devarajegowda, H., Isac, J., Density functional theory study, ft-ir and ft-raman spectra and sqm force field calculation for vibrational analysis of 1, 3-bis (hydroxymethyl) benzimidazolin-2-one. *Spectrochimica Acta Part A: Molecular and Biomolecular Spectroscopy*, **2013**, 114, 432–440.

[15] Kumar, A., Dwivedi, A., Srivastava, A.K., Misra, N., Narayana, B., Samshuddin, S., Sarojini, B., Molecular structures, vibrational spectra, electronic properties, and molecular docking of two pyrazoline derivatives containing 1-carboxamide and 1-carbothioamide: A comparative study. *Polycyclic Aromatic Compounds*, **2017**, 37(4), 267–279.

[16] Zhou, S., You, B., Yao, Q., Chen, M., Wang, Y., & Li, W. DFT studies of structure and vibrational spectra of 4-benzylidene-1-phenyl-2-selenomorpholino-1*H*-imidazol-5(4*H*)-one and its derivatives. *Spectrochimica Acta Part A: Molecular and Biomolecular Spectroscopy,* **2013**, *110*, 333–342.

[17] Nakamura, N., Ichimaru, Y., Kato, K., Sano, M., Kurosaki, H., Hayashi, K., Miyairi, S., Crystal

structure of 5-methoxyindirubin 3′-oxime. *X-ray Structure Analysis Online*, **2020**, 36, 47–48.

[18] Wang, L.-H., Tai, X.-S. The synthesis and crystal structure of two new hydrazone compounds. *Crystals*, **2016**, 6(5), 57.

[19] Ueji, K., Shinozaki, S., Miyamura, K., Crystal structure of the bis [bis (*p*-methoxyphenyl) glyoximato] nickel (II) complex. *X-ray Structure Analysis Online*, **2017**, 33, 71–72.

[20] Takayanagi, H., Ogura, H., Matsuzaki, K., Kitajima, K., Nishimura, T., The crystal and molecular structure of (±)-2-methylamino-4, 5-bis (*p*-chlorophenyl)-4-hydroxy-4 h-imidazole. *Bulletin of the Chemical Society of Japan*, **1979**, 52(11), 3358–3361.

[21] Sologub, O., Rogl, P., Grytsiv, A., & Giester, G., Crystal structure of $R_3Pd_{25-x}B_{8-y}$, R = La, Ce. *Journal of Physics: Conference Series,* **2009**, *176*, 012007.

[22] Shepherd III, J.W., Foxman, B.M., Crystal and molecular structure of an unreactive methacrylate phase, Cu_2 $[C_3H_5COO]$ $_{4.2}$ $[C_3H_5COOH]$. *Molecular Crystals and Liquid Crystals*, **1986**, 137(1), 87–99.

[23] Ghosh, S., Pramanik, S., Mukherjee, A.K. Structure analysis of a phenylpyrazole carboxylic acid derivative crystallizing with three molecules in the asymmetric unit (Z′ = 3) using X-ray powder diffraction. *Powder Diffraction*, **2019**, 34(2), 151–158.

[24] Saeed, A., Khurshid, A., Flörke, U., Echeverría, G. A., Piro, O.E., Gil, D.M., Rocha, M., Frontera, A., El-Seedi, H.R., Mumtaz, A., Erben, M.F. Intermolecular interactions in antipyrine-like derivatives 2-halo-N-(1,5-dimethyl-3-oxo-2-phenyl-2,3-dihydro-1*H*-pyrazol-4-yl)benzamides: X-ray structure, Hirshfeld surface analysis and DFT calculations. *New Journal of Chemistry*, **2020**, 44, 19541–19554.

[25] Prabhuswamy, M., Kumara, K., Pavithra, G., Ajay Kumar, K., Lokanath, N.K. Synthesis, crystal structure and Hirshfeld surface analysis of 5-(3,4-dimethoxyphenyl)-3-(thiophen-2-yl)-4,5-dihydro-1*H*-pyrazole-1-carboxamide. *Chemical Data Collections*, **2016**, 3–4, 26-35.

[26] Haroon, M., Akhtar, T., Yousuf, M., Tahir, M.N., Rasheed, L., Zahra, S.S., Ashfaq, M. Synthesis, crystal structure, Hirshfeld surface investigation and comparative DFT studies of ethyl 2-[2-(2-nitrobenzylidene)hydrazinyl]thiazole-4-carboxylate. *BMC Chemistry*, **2022**, 16, 18.

[27] Kanmazalp, S.D., Dege, N., İlhan, I.O., Akın, N. Crystal structure and Hirshfeld surface analysis of 3,5-bis(4-methoxyphenyl)-4,5-dihydro-1*H*-pyrazole-1-carbothioamide. *Journal of Structural Chemistry*, **2020**, 61(2), 126–132.

[28] Hutchison, G.R., Ratner, M.A., Marks, T.J., Naaman, R., Adsorption of polar molecules on a molecular surface. *The Journal of Physical Chemistry B*, **2001**, 105(15), 2881–2884.

[29] Khan, M.F., Rashid, R.B., Hossain, M.A., Rashid, M.A., Computational study of solvation free energy, dipole moment, polarizability, hyperpolarizability and molecular properties of betulin, a constituent of corypha taliera (roxb.). *Dhaka University Journal of Pharmaceutical Sciences*, **2017**, 16(1), 1–9.

[30] Laidig, K., Bader, R. Properties of atoms in molecules: Atomic polarizabilities. *Journal of Chemical Physics,* **1990**, 93, 7213–7224.

[31] Zhang, P., Bao, P., Gao, J., Dipole preserving and polarization consistent charges. *Journal of Computational Chemistry*, **2011**, 32(10), 2127–2139.

[32] Bhatia, M., An overview of conceptual-dft based insights into global chemical reactivity of volatile sulfur compounds (VSCs). *Computational Toxicology*, **2024**, 29, 100295.

[33] Molski, M., Theoretical study on the radical scavenging activity of gallic acid. *Heliyon*, **2023**, 9(1),

[34] N'dri, J.S., Koné, M.G.-R., Kodjo, C., Kablan, A., Affi, S., Ouattara, L., Ziao, N., Theoretical study of the chemical reactivity of five schiff bases derived from dapsone by the dft method. *Chemical Science International Journal*, **2018**, 22(4), 1–11.

[35] Ji, H.-F., Tang, G.-Y., Zhang, H.-Y. A theoretical study on the structure-activity relationships of metabolites of folates as antioxidants and its implications for rational design of antioxidants. *Bioorganic & Medicinal Chemistry*, **2005,** 13(4), 1031–1036.

[36] Khodaei, M.M., Alizadeh, A., Ghanbari, P., Theoretical study of structural effects on reactivity and stability of isomeric pyrano-, thiopyrano-and selenopyranopyrroles. *Indian Journal of Chemistry*, **2019**, 58(1311–1318.

[37] Jämbeck, J.P., Mocci, F., Lyubartsev, A.P., Laaksonen, A., Partial atomic charges and their impact on the free energy of solvation. *Journal of Computational Chemistry*, **2013**, 34(3), 187–197.

[38] Marahatta, A.B. Computational Study on Electronic Structure, Atomic Charges Distribution and Frontier Molecular Orbitals of Butadiene: General Features for Diels-Alder Reaction. *The International Journal of Progressive Sciences and Technologies*, **2020**, 19, 48–64.

[39] Özbek, F.E.Ö., Uğurlu, G., Kalay, E., Necefoğlu, H., Hökelek, T. Theoretical and experimental assesment of structural, spectroscopic, electronic and nonlinear optical properties of two aroylhydrazone derivative. *Journal of Molecular Structure*, **2021**, 1223, 128982.

[40] Merzouki, O., Arrousse, N., Ech-Chihbi, E., Alanazi, A. S., Mabrouk, E. H., Hefnawy, M., El Moussaoui, A., Touijer, H., El Barnossi, A., Taleb, M. Environmentally Friendly Synthesis of New Mono- and Bis-Pyrazole Derivatives; In Vitro Antimicrobial, Antifungal, and Antioxidant Activity; and In Silico Studies: DFT, ADMETox, and Molecular Docking. *Pharmaceuticals*, **2025**, 18(2), 167.

[41] Rose, Y., Duarte, J.M., Lowe, R., Segura, J., Bi, C., Bhikadiya, C., Chen, L., Rose, A.S., Bittrich, S., Burley, S.K., Rcsb protein data bank: Architectural advances towards integrated searching and efficient access to macromolecular structure data from the pdb archive. *Journal of Molecular Biology*, **2021**, 433(11), 166704.

[42] El-Sayed, H.A., Moustafa, A.H., Farargy, A.F.E., Mohammed, S.M., Saudy, E., Gad, E.M. Novel triazole-, oxadiazole-, and pyrazole-nicotinonitrile hybrids: Synthesis, DFT study, molecular docking, and antimicrobial activity. *Russian Journal of General Chemistry*, **2022**, 92, 709–717.

[43] Kaddouri, Y.A.T., Abrigach, F., El Azzouzi, M., Zarrouk, A., Touzani, R. Synthesis, characterization, reaction mechanism prediction, and biological study of mono-, bis-, and tetrakis-pyrazole derivatives against Fusarium oxysporum f. sp. albedinis: Conceptual DFT and ligand–protein docking studies. *Bioorganic Chemistry*, **2021**, 110, 104696.

HOW TO CITE THIS ARTICLE

N.Q.Q. Savriyeva, M.A. Tursunov, B.S. Ganiev. Novel [5-hdroxy-3-phenyl-5-(trifluoromethyl)-4,5-dihydro-1H-pyrazol-1-yl](phenyl)methanone: Synthesis, Characterization, and Computational Analysis. *Adv. J. Chem. A*, 2026, 9(2), 192-207.

DOI: 10.48309/AJCA.2026.530286.1865
URL: https://www.ajchem-a.com/article_229190.html